BBA - Molecular Basis of Disease 1864 (2018) 1037–1050

2018 china
dl 1/6/2020

Contents lists available at ScienceDirect

BBA - Molecular Basis of Disease

journal homepage: www.elsevier.com/locate/bbadis

Pyridostigmine protects against cardiomyopathy associated with adipose tissue browning and improvement of vagal activity in high-fat diet rats

Yi Lu[a], Qing Wu[a], Long-Zhu Liu[a], Xiao-Jiang Yu[a], Jin-Jun Liu[a], Man-Xiang Li[b], Wei-Jin Zang[a,*]

[a] Department of Pharmacology, School of Basic Medical Sciences, Xian Jiaotong University Health Science Center, Xi'an 710061, Shaanxi, People's Republic of China
[b] Department of Respiratory and Critical Care Medicine, First Affiliated Hospital of Medical Collage, Xian Jiaotong University, Xi'an 710061, Shaanxi, People's Republic of China

ARTICLE INFO

Keywords:
Obesity
Cardiac lipid accumulation
Cardiac remodeling
Pyridostigmine
Adipose tissue

ABSTRACT

Obesity, a major contributor to the development of cardiovascular diseases, is associated with an autonomic imbalance characterized by sympathetic hyperactivity and diminished vagal activity. Vagal activation plays important roles in weight loss and improvement of cardiac function. Pyridostigmine is a reversible acetylcholinesterase inhibitor, but whether it ameliorates cardiac lipid accumulation and cardiac remodeling in rats fed a high-fat diet has not been determined. This study investigated the effects of pyridostigmine on high-fat diet-induced cardiac dysfunction and explored the potential mechanisms. Rats were fed a normal or high-fat diet and treated with pyridostigmine. Vagal discharge was evaluated using the BL-420S system, and cardiac function by echocardiograms. Lipid deposition and cardiac remodeling were determined histologically. Lipid utility was assessed by qPCR. A high-fat diet led to a significant reduction in vagal discharge and lipid utility and a marked increase in lipid accumulation, cardiac remodeling, and cardiac dysfunction. Pyridostigmine improved vagal activity and lipid metabolism disorder and cardiac remodeling, accompanied by an improvement of cardiac function in high-fat diet-fed rats. An increase in the browning of white adipose tissue in pyridostigmine-treated rats was also observed and linked to the expression of UCP-1 and CIDEA. Additionally, pyridostigmine facilitated activation of brown adipose tissue via activation of the SIRT-1/AMPK/PGC-1α pathway. In conclusion, a high-fat diet resulted in cardiac lipid accumulation, cardiac remodeling, and a significant decrease in vagal discharge. Pyridostigmine ameliorated cardiomyopathy, an effect related to reduced cardiac lipid accumulation, and facilitated the browning of white adipose tissue while activating brown adipose tissue.

1. Introduction

Obesity is a complex disease characterized by excessive, abnormal accumulation of body fat and associated with decreased physical activity [1]. As one of the major contributors to an increased risk of cardiovascular disease, including hypertension, stroke and congestive heart failure, obesity has become a global public health concern [2]. Recent studies have shown that animals fed a high-fat diet exhibit an autonomic imbalance characterized by sympathetic hyperactivity [3,4]. Sebastiano et al. reported decreases in body weight and fat in obese rats following vagal nerve stimulation [5]. In clinical trials and our own experimental studies, vagal nerve stimulation improved cardiac function and exerted cardioprotective effects in various cardiovascular diseases [6,7]. Pyridostigmine, a reversible acetylcholinesterase (AChE) inhibitor, protects against cardiac dysfunction by improving vagal activity [8,9]. Our recent studies provided evidence of the protective effect of pyridostigmine on cardiac function, by attenuating cardiac remodeling [10,11]. However, whether pyridostigmine can ameliorate cardiac dysfunction in rats following high-fat diet feeding had not been investigated.

Excess lipid accumulation as a result of increased energy intake and decreased energy expenditure underlies obesity. This pathologic response, together with the over-activation of lipid signaling pathways, results in the accumulation of potentially toxic lipid species, which in turn triggers cellular distress and dysfunction and may ultimately result in apoptotic cell death or lipoapoptosis [12]. A further consequence of excess, abnormal lipid accumulation is the activation of downstream signaling cascades that induce cardiomyocyte apoptosis, resulting in cardiomyopathy [13]. It has been previously suggested that an elevation in myocardial triacylglycerol (TAG) content, which is generally believed to be non-toxic, serves as a biomarker of the increased cardiac content of many toxic lipid metabolites (such as ceramide,

* Corresponding author at: P.O. Box 77#, No.76 Yanta West Road, Department of Pharmacology, Xi'an Jiaotong University Health Science Center, Xi'an 710061, People's Republic of China.
E-mail address: zwj@mail.xjtu.edu.cn (W.-J. Zang).

https://doi.org/10.1016/j.bbadis.2018.01.006
Received 11 October 2017; Received in revised form 22 December 2017; Accepted 4 January 2018
Available online 06 January 2018
0925-4439/ © 2018 Elsevier B.V. All rights reserved.

diacylglycerol and long-chain acyl CoA) that deteriorate cardiac metabolism and function [14]. Pulinilkunnil et al. found that adipose TAG lipase deficiency in diabetic mice increases the levels of TAG and toxic lipid intermediates, causing cardiac diastolic dysfunction. Conversely, the overexpression of adipose TAG lipase was sufficient to attenuate diabetes-induced cardiomyopathy [15].

Adipose tissue expansion induced by excess fat accumulation involves both hypertrophy and hyperplasia, with subsequent lipid overflow and ectopic deposition. This sequence of events may be one of the primary contributors to increased TAG levels and lipid accumulation [16,17]. Humans have two major types of adipose tissue: white adipose tissue (WAT) and brown adipose tissue (BAT) [18]. White adipocytes primarily function to store energy in lipid droplets, in the form of TAG, while brown adipocytes are prominently involved in thermoregulation, by consuming energy in a process associated with an increase in the levels of the protein markers uncoupling protein-1 (UCP-1) and cell death-inducing DNA fragmentation factor A-like effector (CIDEA) [19,20]. Recent studies have shown that a high-fat diet leads to WAT and BAT dysfunction [18]. Meanwhile, inducing the browning of WAT ameliorates high fat diet-induced obesity [21]. Regarding BAT, activation via SIRT-1/AMPK/PGC-1α leads to an increase in energy expenditure by non-shivering thermogenesis [22,23]. Thus, improving WAT browning and BAT activation may protect against cardiomyopathy and improve cardiac function.

This study investigates whether, in high-fat diet-fed rats, pyridostigmine can inhibit cardiomyopathy and improve cardiac function by increasing WAT browning and activating BAT through the SIRT-1/AMPK/PGC-1α signaling pathway.

2. Materials and methods

2.1. Animals

Adult male Sprague-Dawley rats (8–10 weeks old) were supplied by the Experimental Animal Centre of Xi'an Jiao Tong University. All experimental procedures were performed in accordance with the Guide for the Care and Use of Laboratory Animals published by the National Institutes of Health (NIH publication No. 85-23, revised 1996) and approved by the Ethics Committee of Xi'an Jiao tong University.

2.2. Diets

The high-fat diet rat group (HFD) were fed a high-fat diet (45% kcal from fat, 35% from carbohydrates and 20% from protein). While the normal-fat diet rat group (NFD) was fed a normal-fat diet (10% kcal from fat, 70% from carbohydrates and 20% from protein). Both the high-fat diet (Open Source diets D12451) and the normal-fat diet (Open Source diets D12450H) were purchased from Open Source Animal Diets (Changzhou Co., Ltd., Jiangsu, China). All diets were fed daily and rats were allowed to drink water ad libitum.

2.3. Establishment of the diet-induced obesity animal model and drug administration

All rats (n = 80) were randomly assigned to the NFD (n = 40) group or HFD (n = 40) group. The HFD group was fed a high-fat diet for 12 weeks, during which time the NFD group was fed a normal diet. After 12 weeks, the two groups were then randomly divided into the following subgroups: NFD (n = 10), NFD + pyridostigmine (NFD + PYR, n = 10), NFD + pyridostigmine + atropine (NFD + PYR + ATRO, n = 10), NFD + nicotinic acid (NFD + NI, n = 10), HFD (n = 10), HFD + pyridostigmine (HFD + PYR, n = 10), HFD + pyridostigmine + atropine (HFD + PYR + ATRO, n = 10), HFD + nicotinic acid (HFD + NI, n = 10). Pyridostigmine (31 mg/kg/day) (Shanghai Zhongxi Sunve Pharmaceutical Co. Ltd., Shanghai, China) and nicotinic acid (100 mg/kg/day) (Shanghai SINE Pharmaceutical Co. Ltd., Shanghai, China) were administered once per day for 12 weeks. Atropine (0.6 mg/kg/day) (Sigma, St Louis, MO, US) was administered by intraperitoneal injection before pyridostigmine (31 mg/kg/day) once per day for 12 weeks. The body weight and food intake of the rats were recorded weekly for 24 weeks. In addition, the Lee's index was also recorded at 12 and 24 weeks. The Lee's index is used to evaluate the degree of obesity and to assess whether the obesity model is established [24]. We measured the body weight and length of rats in all groups and calculated the Lee's index (Lee's index = body weight $(g)^{1/3} \times 1000$/naso-anal length (cm)) [25].

2.4. Echocardiographic methods

Transthoracic echocardiograms were used to assess cardiac function in all groups at week 24. Briefly, the rats were anesthetized with 1.5–2% isoflurane using a Vevo 2100 high-resolution in vivo imaging system (Visual Sonics Vevo 2100; Visual Sonics Inc., Toronto, Canada) and then placed on a heating pad for transthoracic echocardiography. Heart rate (HR), left ventricular internal dimension in systole and diastole (LVIDs and LVIDd, respectively), the thickness of the interventricular septum in systole and diastole (IVSs and IVSd, respectively) and the thickness of the LV posterior wall in systole and diastole (LVPWs and LVPWd, respectively) were obtained from the echocardiograms. The LV ejection fraction (EF), LV fractional shortening (FS), and end-systolic and end-diastolic LV volume (LVEDV and LVESV, respectively) were calculated according to the traditional formulas.

2.5. Recording of vagal nerve discharge

The whole vagal discharge was recorded and analyzed 24 weeks after treatment using a BL-420S biological signal analytical system (Taimeng Technology Co., Ltd., Chengdu, China). In brief, all rats were anesthetized with pentobarbital sodium (45 mg/kg, i.p.). The right cervical vagus nerve was identified and immersed in warm (37 °C) paraffin (Xian Chemical Industry, Xian, China). Silver electrodes connected to the BL-420S biological signal analytical system for recording vagal discharge were attached to the vagus nerve, and the reference electrode to a skin fold. The settings for the neural discharge patterns were: scanning speed (100 ms/div), power gain (200 μV), time constant, (0.001 s), and frequency filtering (1 KHz). Vagal nerve discharge was integrated and quantified as μvolts × seconds (μV·s). Integrated vagal activity was evaluated as the ratio between integrated vagal discharges in the various groups versus the NFD group. Vagal discharges measured after a 30-min steady-state condition were considered significant.

2.6. Hemodynamic parameters

Hemodynamics were measured and analyzed using the BL-420S biological signal analytical system (Taimeng Technology Co., Ltd.). The right carotid artery was isolated and pressure transducers were introduced into the left ventricle to measure mean arterial pressure (MAP), LV systolic pressure (LVSP), LV end-diastolic pressure (LVEDP), and the maximum slope of systolic and diastolic pressure decrements (+ dp/dt and − dp/dt, respectively). All hemodynamic parameters measured after a 30-min steady-state condition were considered significant.

2.7. Preparation of blood and tissue samples

At the end of the experiments, non-fasted rats were euthanized by injecting 1 ml 60 mM KCl (i.v.) [26,27]. Blood samples were collected from the abdominal aorta and centrifuged at 5000 × *g* for 10 min. The serum was then aspirated for further analysis.

The whole heart was quickly arrested and washed with cold phosphate-buffered saline (PBS;137 mM NaCl, 2.7 mM KCl, 10 mM

Na_2HPO_4, and 2 mM KH_2PO_4 at pH 7.4), as described previously [11]. Cardiac tissue was snap-frozen in liquid nitrogen and stored at − 80 °C. The paracardial fat (WAT) and interscapular fat (BAT) were isolated and washed with cold PBS, removing all of the connective tissues [28]. The adipose tissues were also immediately snap-frozen in liquid nitrogen and stored at − 80 °C.

2.8. Serum analyses

AChE activity, the acetylcholine (ACh) level (Jiancheng Bioengineering Institute, Nanjing, China), leptin, ghrelin (Elisa Biotech Co., Ltd., Shanghai, China), and TAG concentrations (Changchun Huili Biotech Co., Ltd., Changchun, China) in plasma samples were measured using commercially available kits according to the manufacturer's instructions.

2.9. Histology

The heart and adipose tissue was excised, washed, and fixed with 4% formalin. Transverse 5-μm-thick sections were cut from paraffin-embedded LV and adipose slices. The tissue sections were stained with hematoxylin and eosin (HE) and Masson's trichrome stains. Myocyte and adipocyte cross-sectional diameter and the fibrosis area were measured using Image-Pro Plus 6.0 (Media Cybernetics, Silver Spring, MD, USA). Fibrosis area percentages were calculated as the ratios between interstitial collagen deposition in the various groups versus the NFD group.

Cardiac lipid accumulation was measured qualitatively in a serial 5-μm frozen section that was stained with Oil Red O (Heart Biological Technology Co., Ltd., Xian, China). Briefly, cardiac tissue was immersed in liquid nitrogen and subsequently stored at − 80 °C. Frozen cardiac tissue was embedded in optimal cutting temperature compound (Sakura Finetek USA, Inc., Torrance, CA, USA) and snap frozen. A cryostat was used to cut tissue sections 5 μm in thickness and the sections were mounted on slides with five sections per slide. Next, cardiac tissue sections were fixed in 4% formaldehyde, washed with 60% isopropyl alcohol and incubated with Oil Red O staining solution at 60 °C 15 min. The sections were then gently washed with Mayer's hematoxylin solution (Heart Biological Technology Co., Ltd.). Neutral lipid accumulation was based on the ratio between the intensity of lipid deposition in the various groups versus the NFD group.

Immunohistochemical staining was used to investigate levels of UCP-1 (#14670; Cell Signaling Technology, Inc., Beverley, MA, USA) and CIDEA (#Ab151577; Abcam, Cambridge, UK) levels in WAT, as well as ceramide (#ALX-804-196; Enzo Life Sciences, Inc., Farmingdale, NY, US) levels in LV tissue according to the manufacturer's instructions.

2.10. RNA extraction and quantitative polymerase chain reaction (PCR) analysis

Total RNA was isolated and extracted from LV tissue and WAT using TRNzol Universal (#DP424; TIAN Biotech Co., Ltd., Beijing, China) according to the manufacturer's protocol. A kit (#A5001; Promega Biotech Co., Ltd., Beijing, China) was used to perform first strand cDNA synthesis according to the procedure recommended by the manufacturer. Quantitative PCR was performed on a TL998-IV PCR detection system (Xi'an Tianlong Science And Technology Co., Ltd., Xi'an, China). β-actin was used as the invariant control. The sequences of the quantitative PCR primers are shown in Table 1. The PCR products were separated and visualized using an image recording system (JS-380C, Shanghai Peiqing Science And Technology Co., Ltd., Shanghai, China). The target bands were quantified by densitometry using Quantity One software (Bio-Rad Laboratories, Hercules, CA, USA). The relative expression levels of mRNA of individual gene was calculated after normalizing to their corresponding β-actin mRNA.

Table 1
Primer sequences in quantitative PCR.

Gene	Forward primer sequence (5′-3′)	Reverse primer sequence (5′-3′)
CD36	TCCTATTGGGAAAGTTATTGCG	AAAGAACCTCAGTGTTCGAGAC
PLIN5	AGGGCTACTTTGTGCGTCTG	GTGTTTGCTCTCCCTCAGTTTC
PLIN1	GAGACCCACATCATTTCTAAGGC	CCCCTTAAAACCTGACTGTGATG
PKCβ	GACAACAATGGCAACAGGGAC	CATCTTTCTTCAGGATCTTCACG
PPARα	TCTGAAAGATTCGGAAACTGC	GTTGCTAGTCTTTCCTGCGAG
mtDNA	GGTTCTTACTTCAGGGCCATC	TGATTAGACCCGTTACCATCG
mtTFA	CTGTCAGCCTTATCTGTATTCC	CTTTTGCATCTGGGTGTTTAG
β-actin	TGTGACGTTGACATCCGTAAAG	TAGGAGCCAGGGCAGTAATC

CD36: cluster of differentiation 36; PLIN5: perilipin 5; PLIN1: perilipin 1; PKCβ: Protein kinase Cβ; PPARα: peroxisome proliferator-activated receptor α; mtDNA: mitochondrial DNA; mtTFA: mitochondrial transcription factor A.

2.11. Western blot analysis

BAT protein samples (30 μg) were separated by sodium dodecyl sulfate polyacrylamide gel electrophoresis (SDS-PAGE) on a 10% polyacrylamide gel and transferred to a PVDF membrane (Millipore, Billerica, MA). The membranes were incubated for 1 h at room temperature in a blocking solution of Tris-buffered saline containing 0.1% Tween (TBST) and 5% bovine serum albumin, and then with the following primary antibodies: mouse monoclonal SIRT-1 (#8469; Cell Signaling Technology, Inc.), rabbit polyclonal AMPKα (#2532; Cell Signaling Technology), rabbit polyclonal phosphor-AMPKα (#2531; Cell Signaling Technology), PGC-1α (#2178; Cell Signaling Technology), rabbit monoclonal UCP-1 (Cell Signaling Technology), rabbit polyclonal CIDEA (Abcam) and mouse monoclonal GAPDH (#AT0002; Cell Signal Pathway Research Tools Supplier, Inc., WI). After incubating with primary antibodies, the membrane was washed with TBST and then incubated for 35 min with peroxidase-conjugated rabbit anti-mouse IgG (#L3032-2; Signalway Antibody LLC, College Park, MD, USA), and goat anti-rabbit IgG (#ZB-5301; ZSGB-BIO, Beijing, China). Chemiluminescence was detected using an ECL-Plus kit (Millipore Billerica, MA, USA) and exposure to X-ray film. Bands were quantified by densitometry using Quantity One software (Bio-Rad Laboratories).

2.12. Statistical analysis

The data are expressed as means ± standard error of the mean. For statistical analysis, the data were analyzed using one-way ANVOVA followed by Tukey's multiple comparison test (eight groups). Student's *t*-test for comparisons was applied for comparison of two groups (NFD vs. HFD). A p value < 0.05 was considered statistically significant.

3. Results

3.1. Effects of a high-fat diet on body weight and vagal nerve activity

Body weight and Lee's index were significantly increased in HFD rats compared with NFD rats in the first 12-week dietary intervention, which indicated that the obesity model was established (Fig. 1A, B and E). During the second 12-week dietary intervention, body weight gain was higher in the HFD than in the NFD group (Fig. 1A, B). Food and energy intake increased substantially in HFD compared with NFD rats (Fig. 1C, D). Lee's index was also moderately higher in HFD than in NFD rats (Fig. 1E).

Vagal nerve discharge was recorded using the BL-420S biological signal analytical system (Fig. 1F, G). Rats in the HFD group had lower levels of vagal discharge and serum ACh than rats in the NFD group (Fig. 1H, J). Serum AChE activity was higher in HFD than NFD rats (Fig. 1I).

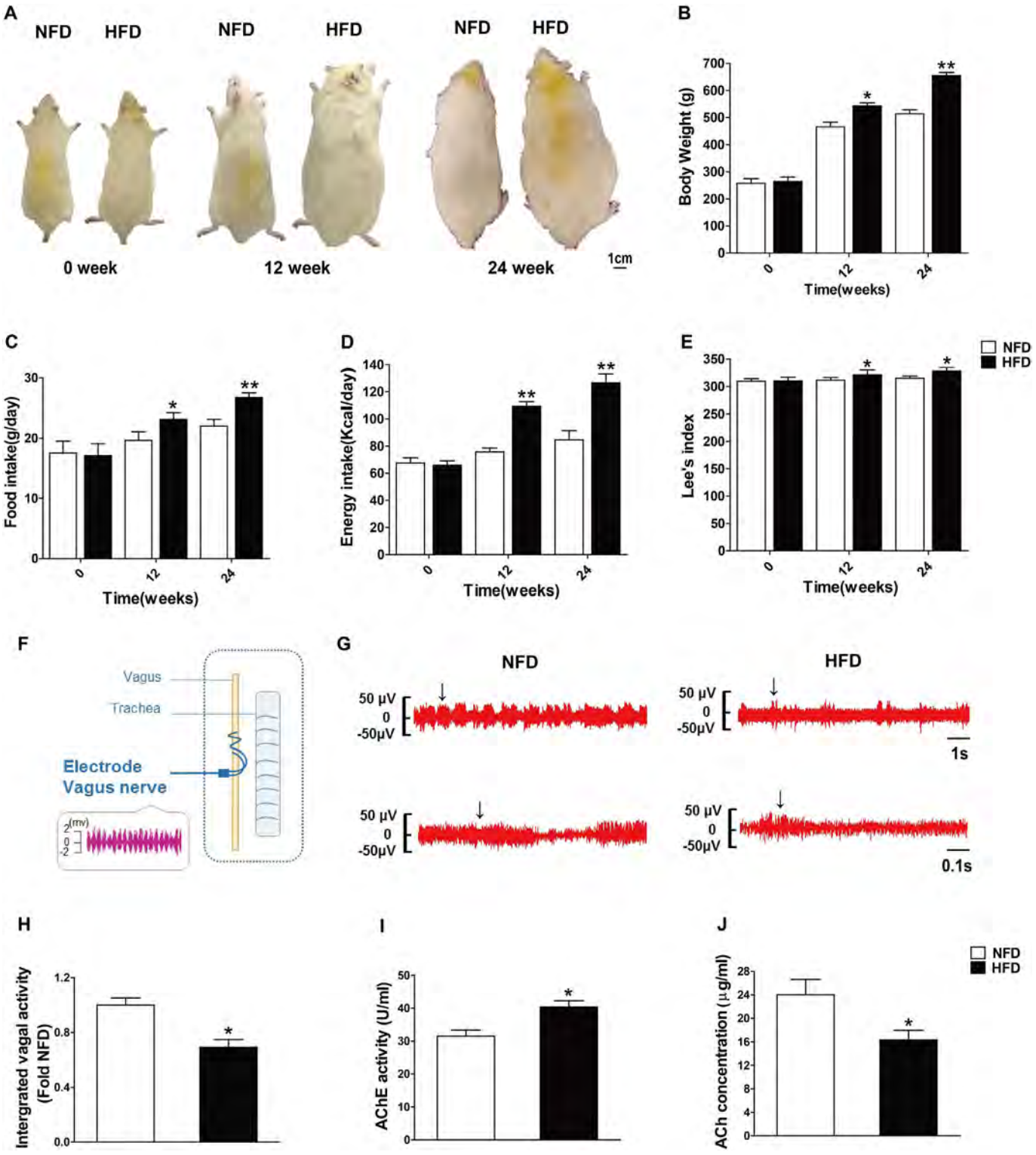

Fig. 1. Effect of a high-fat diet on body weight gain in high-fat diet-fed rats. (A) Representative images of rats fed either a high-fat or normal-fat diet. (B–E) Body weight, food intake, energy intake and Lee's index in high-fat diet group (HFD) and normal-fat diet group (NFD) rats. (F) Vagal nerve discharge recording. (G) Representative tracings of a high-fat diet on vagal nerve discharge. (H) Integrated recording of vagal nerve discharge in high-fat diet-fed rats. (I, J) Serum acetylcholinesterase (AChE) activity and the acetylcholine (ACh) concentration in HFD or NFD rats. Data are represented as means ± standard error of the mean (n = 8). $^{*}p < 0.05$, $^{**}p < 0.01$ vs. NFD rats.

3.2. Increased lipid accumulation in rats fed a high-fat diet

The diameter of white and brown adipocytes was markedly increased in rats of the HFD group (Fig. 2A–D). Cardiac lipid deposition was significantly increased in HFD rats (Fig. 2E, F). Higher levels of serum TAG (Fig. 2I), PKCβ mRNA (Fig. 2J), and ceramide (Fig. 2G, H) were also observed in the HFD group.

3.3. Effect of pyridostigmine on body weight and vagal nerve activity in HFD rats

As shown in Fig. 3, progressive increases in body weight, food

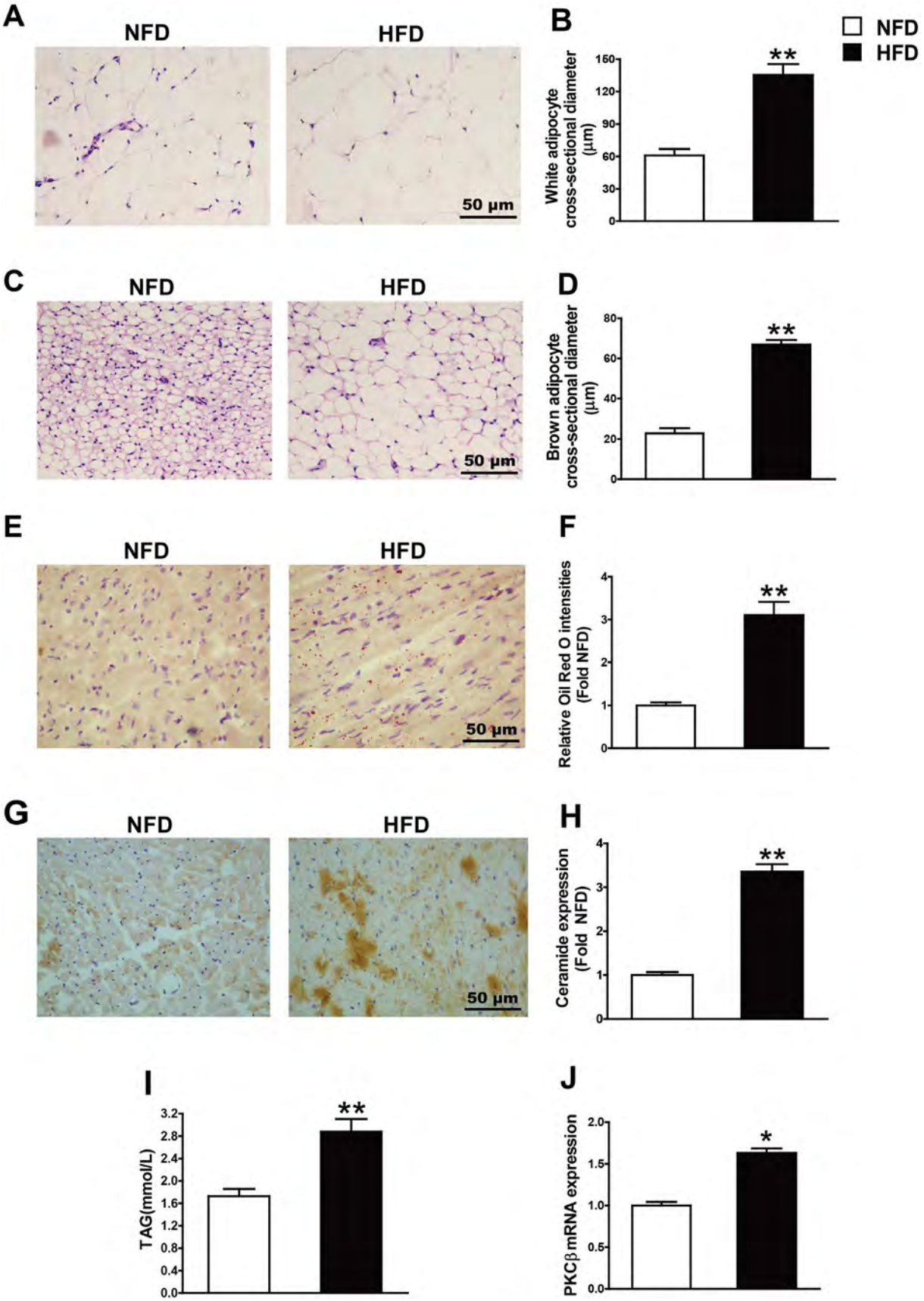

Fig. 2. A high-fat diet for 24 weeks led to adipose tissue dysfunction and lipid accumulation in rats. (A, C) Representative hematoxylin and eosin (HE) staining of white and brown adipose tissue (WAT and BAT, respectively). (B, D) Cross-section of adipocytes in WAT and BAT. (E) Representative Oil Red O staining of left ventricular lipid deposition in the left ventricle. (F) Quantification of Oil Red O staining. (G) Representative immunohistochemical staining of ceramide in the left ventricle. (H) Quantification of ceramide level in the left ventricle. (I) Serum TAG level. (J) PKCβ mRNA level in the left ventricle. Data are represented as means ± standard error of the mean (n = 8). $^{*}p < 0.05$, $^{**}p < 0.01$ vs. NFD.

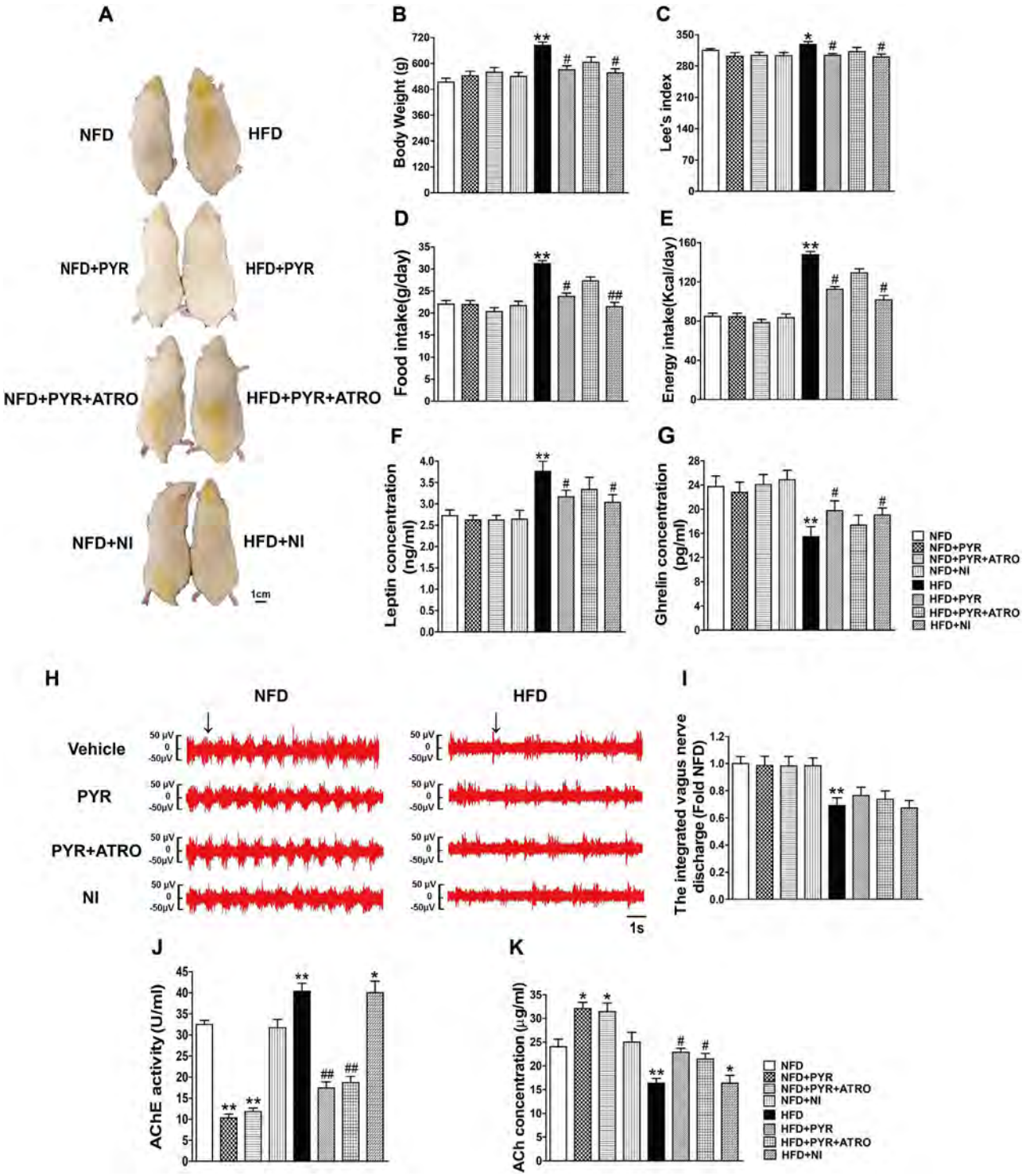

Fig. 3. Pyridostigmine treatment for 12 weeks decreases body weight in high-fat diet-fed rats. (A) Representative images of rats treated with pyridostigmine. (B–E) The effect of pyridostigmine on body weight, Lee's index, food intake and energy intake in all rats. (F, G) Serum leptin and ghrelin concentration. (H) Representative images of pyridostigmine on vagal nerve discharge. (I) Integrated vagal nerve discharge in all groups. (J, K) Serum AChE activity and ACh concentration. Data are represented as means ± standard error of the mean (n = 8). $^{*}p < 0.05$, $^{**}p < 0.01$ vs. NFD; $^{\#}p < 0.05$, $^{\#\#}p < 0.01$ vs. HFD.

intake, energy intake and Lee's index were determined in high-fat diets-fed rats (Fig. 3A–E). Pyridostigmine treatment reduced body weight, energy intake and Lee's index in HFD, but not in NFD, rats at 24 weeks (Fig. 3A–E). In addition, serum leptin and ghrelin levels were also evaluated in all groups. Serum leptin concentration increased, while ghrelin level decreased, in HFD compared with NFD rats; these outcomes were reversed by pyridostigmine (Fig. 3F, G). To further explore the potential mechanisms of pyridostigmine, a reversible AChE inhibitor, non-selective muscarine (M) ACh receptor blocker (atropine) was administered by intraperitoneal injection prior to pyridostigmine administration in the HFD + PYR + ATRO group. In the HFD rats, atropine partly abolished the effect of pyridostigmine on body weight, food intake, energy intake, Lee's index, leptin and ghrelin levels.

In the present study, nicotinic acid was used a positive control drug.

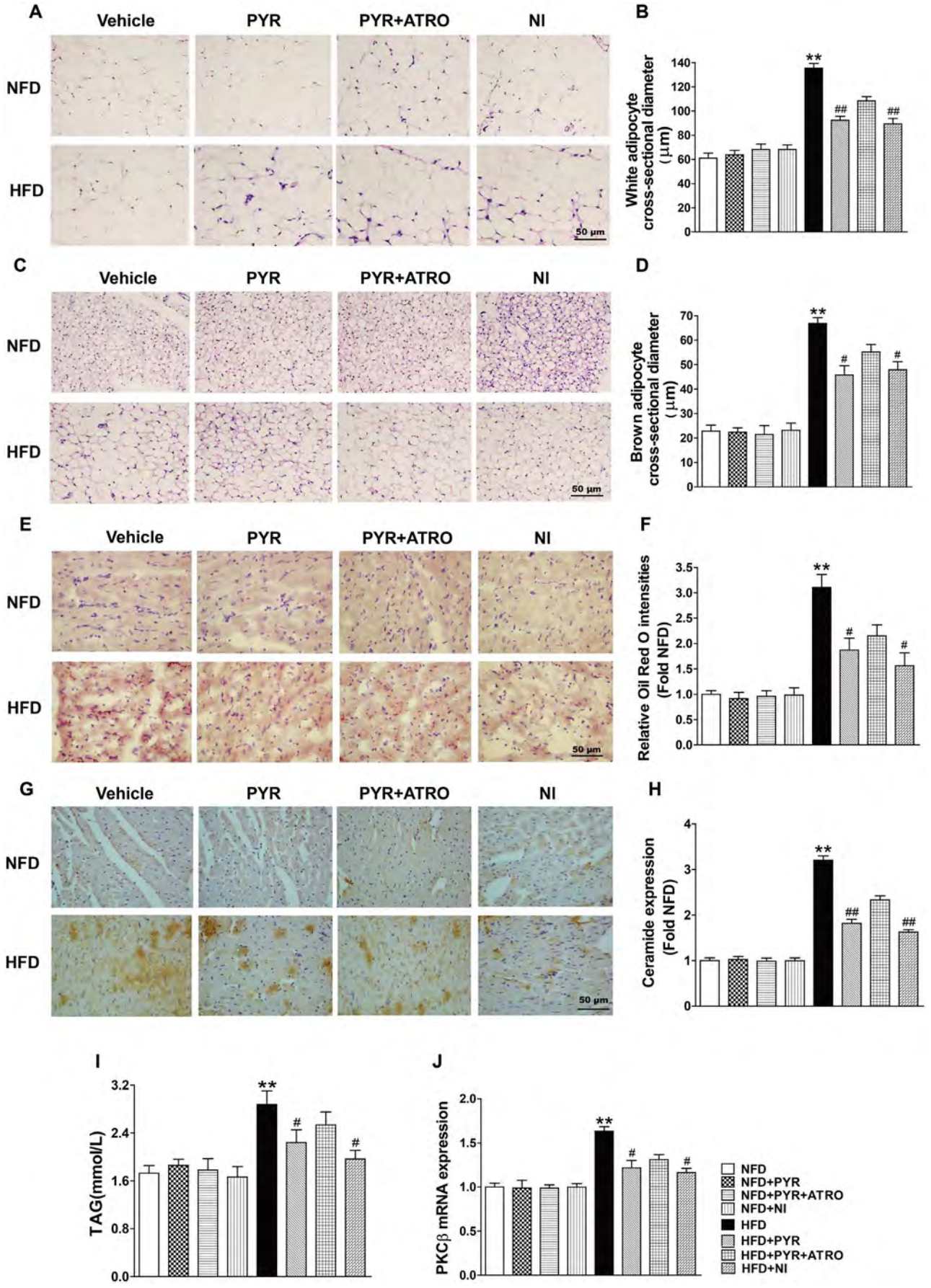

(caption on next page)

Fig. 4. Lipid accumulation is reduced in HFD rats treated with pyridostigmine for 12 weeks. (A, C) Representative HE-stained WAT and BAT sections from all groups. (B, D) The effect of pyridostigmine on adipocytes from WAT and BAT, as seen in cross-section. (E) Representative left ventricular sections stained with Oil Red O. (F) Quantification of Oil Red O staining. (G) Representative immunohistochemical staining of ceramide. (H) Quantification of ceramide levels in the left ventricle. (I) Serum TAG levels. (J) PKCβ mRNA levels in the left ventricle. Data are represented as means ± standard error of the mean (n = 8). $^{*}p < 0.05$, $^{**}p < 0.01$ vs. NFD; $^{\#}p < 0.05$, $^{\#\#}p < 0.01$ vs. HFD.

Given that nicotinic acid also exerts important cardioprotection effects by reducing TAG level directly, we investigated differences in effects and mechanisms between pyridostigmine and nicotinic acid. Our results showed that nicotinic acid also decreased body weight, energy intake, Lee's index, leptin and ghrelin levels in HFD rats.

Recordings of the spontaneous discharges of the vagus nerve, as measured in the tested groups at 24 weeks, are presented in Fig. 3. Vagal discharge was remarkably lower in HFD than in NFD rats (Fig. 3H, I) and neither pyridostigmine nor pyridostigmine + atropine or nicotinic acid affected vagal nerve discharge in any of the groups.

To further determine the effect of pyridostigmine on vagal activity in high-fat diet-fed rats, serum levels of ACh and AChE were measured. As shown in Fig. 3, the serum concentration of ACh was significantly reduced in HFD rats. Treatment with pyridostigmine, but not nicotinic acid, increased the serum ACh concentration in both the NFD + PYR and the HFD + PYR groups (Fig. 3K). By contrast, AChE activity was significantly lower in rats treated with pyridostigmine than in untreated rats (Fig. 3J). Nicotinic acid had no effect on AChE activity in the NFD + NI and HFD + NI groups, and atropine did not attenuate the effect of pyridostigmine on either serum AChE activity or the ACh concentration.

3.4. Pyridostigmine reduced cardiac lipid accumulation in HFD rats

The increase in adipocyte diameter determined in HFD rats was inhibited by pyridostigmine or nicotinic acid treatment (Fig. 4A–D), which also improved adipose function.

Oil Red O staining and immunochemistry staining showed that the accumulation of lipid and ceramide was significantly higher in HFD than in NFD rats (Fig. 4E–H). Both biomarkers were suppressed by pyridostigmine and nicotinic acid. Similarly, serum TAG and PKCβ mRNA levels were much higher in the HFD than in the NFD group (Fig. 4I, J) but were lowered by pyridostigmine or nicotinic acid treatment.

3.5. Pyridostigmine ameliorated cardiac remodeling in rats on a high-fat diet

Lipid uptake (cluster of differentiation 36, CD36), lipid storage (perilipin 5, PLIN5), and fatty acid oxidation (peroxisome proliferator-activated receptor α, PPARα) play critical roles in preserving cardiac function. A high-fat diet led to a marked increase in CD36 mRNA, and a significant reduction in PLIN5 mRNA and PPARα mRNA levels (Fig. 5E–G). Pyridostigmine or nicotinic acid improved lipid uptake, lipid storage, and fatty acid oxidation in HFD + PYR rats. In addition, histopathological studies revealed a larger cardiomyocyte diameter, and greater interstitial fibrosis, in HFD than in NFD rats (Fig. 5A–D). However, both were significantly attenuated by pyridostigmine or nicotinic acid. In HFD rats, pyridostigmine was more effective than nicotinic acid in reducing collagen deposition, whereas the effect of atropine was only partial. There was no significant difference in the cardiac histopathology of NFD rats treated versus not treated with either drug.

3.6. Pyridostigmine attenuated cardiac dysfunction in high-fat diet-fed rats

Cardiac hypertrophy induced by a high-fat diets is associated with an increase in ventricular wall thickness [IVSd(s), LVPWd(s)] and ventricular volume [LVIDd(s), LVED(S)V]. Echocardiography studies showed that LVIDd(s), LVED(S)V, IVSd(s), and LVPWd(s) were markedly increased in the HFD group. In addition, EF and FS decreased significantly in HFD rats (Table 2) but both of the cardiac function indexes were reversed by treatment with pyridostigmine or nicotinic acid. Atropine did not significantly abolish the protective effect of pyridostigmine. Treatment with pyridostigmine, pyridostigmine + atropine or nicotinic acid did not abolish the effect on cardiac function in NFD rats. In the HFD groups, there were significant increases in MAP, LVSP and LVEDP, and a decrease in ± dp/dt (Table 2), whereas pyridostigmine or nicotinic acid decreased MAP, LVSP and LVEDP and increased ± dp/dt, leading to improved hemodynamic parameters. The protective effect of pyridostigmine was not abolished totally by an intraperitoneal injection of atropine before pyridostigmine administration. No changes in hemodynamic profiles were observed in the NFD + PYR, NFD + PYR + ATRO, or NFD + NI groups compared to the NFD group. In addition, HR was comparable between groups.

3.7. Pyridostigmine treatment enhances WAT browning and BAT activation

To investigate the potential mechanisms of pyridostigmine action, the levels of UCP-1 and CIDEA, as well as CD36 mRNA, PLIN1 mRNA, and PPARα mRNA in WAT were investigated immunohistochemically and by PCR analysis, respectively. As shown in Fig. 6, pyridostigmine or nicotinic acid increased the levels of UCP-1 and CIDEA, and improved lipid uptake, lipid storage, and fatty acid oxidation in WAT (Fig. 6A–I). Meanwhile, treatment with pyridostigmine or nicotinic acid increased mitochondrial DNA (mtDNA) and mitochondrial transcription factor A (mtTFA) mRNA levels (Fig. 6H, I). Additionally, the expression of SIRT-1, AMPK, PGC-1α, UCP-1, and CIDEA, as well as the levels of phosphorylated AMPK (p-AMPK), were evaluated by western blot analysis in BAT. The expression of SIRT-1, PGC-1α, CIDEA, UCP-1 and p-AMPK, but not of total AMPK, was significantly lower in the BAT of HFD than of NFD rats (Fig. 6J–O). Treatment with pyridostigmine or nicotinic acid reversed these changes in the HFD + PYR and HFD + NI groups, respectively. Atropine did not fully block the effect of pyridostigmine. In NFD rats, there were no marked changes in CD36, PLIN1, PPARα, SIRT-1, p-AMPK, PGC-1α, CIDEA or UCP-1 levels.

4. Discussion

Obesity is accompanied by a cardiac lipid metabolism disorder, leading to accumulation of potentially toxic lipid species and thus an increased risk of cardiovascular disease. The inhibition of cardiac lipid accumulation may protect against cardiac dysfunction in obesity. This study evaluated the effect of pyridostigmine on vagal activity, cardiac lipid accumulation, and cardiac function in high-fat diet-fed rats. The main findings of this study were as follows: (i) a long-term high-fat diet led to the accumulation of several lipid intermediates related to cardiac toxicity, including TAG and ceramide, which were associated with the activation of lipid signaling pathways, as well as a remarkable reduction in vagal discharge; these changes ultimately resulted in cardiac dysfunction and hemodynamic impairment; (ii) pyridostigmine increased the level of ACh by inhibiting AChE activity and reducing the excess deposition of lipid, without affecting vagal discharge; it also attenuated cardiac remodeling, as evidenced by the improvement of lipid utility and the decrease in cardiac hypertrophy and fibrosis; and (iii) pyridostigmine enhanced WAT browning associated with enhanced lipid uptake, lipid storage, and fatty acid oxidation, and also enhanced BAT activation via up-regulation of the SIRT-1/AMPK/PGC-1α signaling cascade (Fig. 7). Thus, browning of adipose tissue may be a novel target for cardioprotection, and improvement of vagal activity by

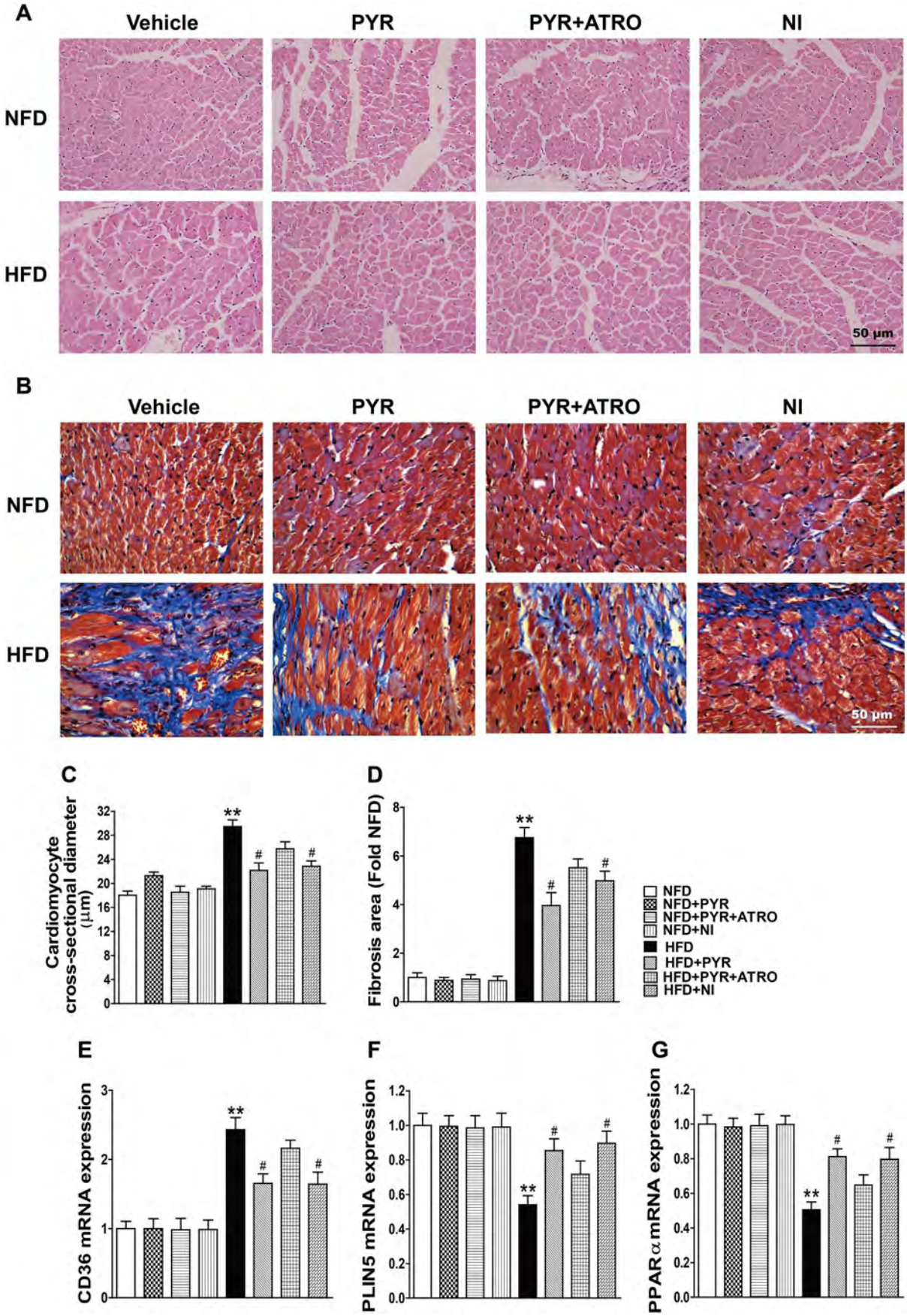

Fig. 5. Pyridostigmine attenuates cardiac remodeling in HFD rats. (A, B) Representative HE and Masson staining sections of left ventricular tissue from all groups. (C, D) The effect of pyridostigmine on cardiomyocytes and the area of fibrosis in the left ventricle, as seen on cross-section. (E, F, G) CD36, PPARα, and PLIN5 mRNA levels in the left ventricle. Data are represented as means ± standard error of the mean (n = 8). $^{*}p < 0.05$, $^{**}p < 0.01$ vs. NFD; $^{\#}p < 0.05$ vs. HFD.

Table 2
Echocardiographic and hemodynamic measurements in HFD rats treated with or without pyridostigmine.

		NFD	NFD + PYR	NFD + PYR + ATRO	NFD + NI	HFD	HFD + PYR	HFD + PYR + ATRO	HFD + NI
Echocardiographic parameters	EF(%)	71.31 ± 3.17	67.83 ± 3.51	68.32 ± 4.40	69.62 ± 3.74	49.48 ± 3.05*	60.83 ± 2.08#	58.30 ± 3.27	59.19 ± 2.87#
	FS(%)	41.94 ± 2.63	38.95 ± 2.70	39.33 ± 3.53	40.39 ± 2.10	26.27 ± 2.08*	33.81 ± 1.72#	32.06 ± 2.92	33.24 ± 2.00#
	HR(bpm)	375.80 ± 16.58	369.08 ± 16.35	385.50 ± 18.64	357.5 ± 15.56	401.43 ± 16.90	411.83 ± 17.31	394.14 ± 14.87	400.75 ± 14.81
	LVIDd(mm)	7.04 ± 0.39	7.24 ± 0.40	7.22 ± 0.34	7.18 ± 0.44	8.86 ± 0.27*	7.85 ± 0.20#	8.26 ± 0.34	7.91 ± 0.22#
	LVIDs(mm)	4.10 ± 0.28	4.42 ± 0.23	4.38 ± 0.31	4.28 ± 0.22	6.53 ± 0.23*	5.26 ± 0.19#	5.61 ± 0.24	5.33 ± 0.20#
	LVEDV(μl)	258.33 ± 20.67	275.57 ± 18.25	273.86 ± 19.50	270.46 ± 23.64	432.37 ± 16.04*	330.83 ± 18.29#	370.07 ± 20.37	336.54 ± 19.56#
	LVESV(μl)	74.96 ± 11.36	88.63 ± 13.82	86.75 ± 11.18	82.16 ± 9.75	218.42 ± 15.41*	133.11 ± 11.70#	154.42 ± 15.56	137.37 ± 15.9#
	LVPWd(mm)	1.74 ± 0.16	1.72 ± 0.12	1.68 ± 0.11	1.69 ± 0.17	2.42 ± 0.13*	1.82 ± 0.10#	1.97 ± 0.18	1.80 ± 0.11#
	LVPWs(mm)	2.71 ± 0.24	2.67 ± 0.26	2.72 ± 0.18	2.77 ± 0.18	3.52 ± 0.12*	2.81 ± 0.13#	2.98 ± 0.17	2.85 ± 0.11#
	IVSd(mm)	1.79 ± 0.23	1.80 ± 0.12	1.78 ± 0.18	1.75 ± 0.08	2.48 ± 0.10*	1.82 ± 0.15#	2.07 ± 0.14	1.84 ± 0.16#
	IVSs(mm)	2.46 ± 0.15	2.44 ± 0.21	2.58 ± 0.20	2.41 ± 0.17	3.22 ± 0.17*	2.54 ± 0.14#	2.93 ± 0.14	2.58 ± 0.12#
Hemodynamic data	MAP	106.9 ± 5.0	103.7 ± 4.1	108.2 ± 3.9	108.3 ± 4.8	136.6 ± 4.6*	110.8 ± 4.1#	122.2 ± 5.5	116.5 ± 3.9#
	LVSP	125.7 ± 3.8	123.4 ± 3.2	122.2 ± 3.5	124.0 ± 3.9	154.0 ± 4.7*	132.5 ± 3.6#	143.7 ± 5.8	133.4 ± 3.8#
	LVEDP	13.36 ± 1.20	14.29 ± 1.69	15.76 ± 1.81	14.44 ± 1.80	27.79 ± 2.19*	19.09 ± 1.35#	21.66 ± 2.43	19.08 ± 1.93#
	+ dp/dt	7776 ± 245	7761 ± 321	7911 ± 224	7819 ± 302	6628 ± 186*	7548 ± 165#	7148 ± 170	7587 ± 240#
	− dp/dt	7212 ± 139	7156 ± 144	7154 ± 150	7111 ± 145	6026 ± 153*	6835 ± 115#	6360 ± 198	6702 ± 166#

EF, left ventricular ejection fraction; FS, left ventricular fractional shortening; HR, heart rate; LVIDd(s), left ventricular internal dimension in systole and diastole; LVED(S)V, end-systolic and end-diastolic left ventricular volumes; IVSd(s), thickness of the interventricular septum; LVPWd(s), thickness of the left ventricular posterior wall in systole and diastole. MAP: mean arterial pressure; LVSP: left ventricular pressure; LVEDP: left ventricular end-diastolic pressure; ± dp/dt: maximum slope of systolic pressure increment and diastolic pressure decrement. Data are shown as the mean ± standard errors of the mean (n = 8). *$p < 0.05$ vs. NFD. #$p < 0.05$ vs. HFD; #$p < 0.05$ vs. HFD.

pyridostigmine could be a new therapeutic strategy to alleviate cardiac dysfunction related to obesity.

Previous clinical studies have shown that a high-fat diet leads to cardiac dysfunction which is associated with autonomic imbalance characterized by hyperactivity of the sympathetic nervous system [29,30]. Laiali et al. found that diet-induced obesity increased sympathetic activity in mice with obesity-associated hypertension [3]. Inhibition of sympathetic nerve activity reduces inflammation following renal denervation in obese rats [31]. These results suggested that restoring autonomic balance, either by reducing an enhanced sympathetic activity or increasing vagal nerve activity, is an important potential therapeutic strategy in the obese. A recent study showed that vagal nerve stimulation reduced both lipid deposition and body weight in obese rats [5,32]. In addition to improved vagal nerve activity via direct vagal stimulation, animal models of cardiovascular disease were used to demonstrate that cardiac dysfunction can be attenuated by pharmacological modulation and exercise training [33]. Improvement of vagal activity may play an important role in reducing the cardiac dysfunction induced by obesity. Most studies have shown that pyridostigmine, a reversible anticholinesterase agent, protects against cardiovascular diseases by improving vagal activity [8,34]. Therefore, pyridostigmine may offer a novel approach to inhibiting cardiac dysfunction in obesity.

An association between vagal nerve stimulation and weight loss in patients with refractory epilepsy was reported; the mechanism included a decrease in food craving [35,36]. A recent study similarly showed that vagal nerve stimulation inhibits body weight and fat mass gain, also via a reduction in food intake [5]. In the present study, body weight, food intake, energy intake, Lee's index, serum leptin, and ghrelin concentration differed significantly between NFD and HFD rats. Treatment of HFD-fed rats with pyridostigmine (HFD + PYR group) reduced all of these parameters. The vagus nerve, as the major neuroanatomic substrate in the intestinal-tract-brain axis, transmits signals induced by food in the gastrointestinal tract to sites in the central nervous system, and thus mediated ingestive behavior. Schwartz et al. showed that the intestinal hormone cholecystokinin suppressed food intake by activating the vagal nerve [37]. Meanwhile, Gil et al. found that vagus nerve stimulation had regulatory effects on serum ghrelin and leptin levels in rats fed a high-fat diet, and led to reductions in food intake [38]. Therefore, pyridostigmine may affect appetite hormones and inhibit food intake via vagal nerve activation.

The data presented here provide the first direct evidence that vagal discharge was markedly reduced in an animal model of obesity. Pyridostigmine increased serum ACh levels via inhibition of AChE activity, without affecting vagal discharge, consistent with the findings of our previous study [11]. Pyridostigmine, a reversible cholinesterase inhibitor, has a quaternary carbamine group and poorly crosses the blood-brain barrier [39]. Instead, its site of action is the peripheral synaptic cleft, where it increases ACh levels by decreasing AChE activity. This mechanism suggests direct effects of pyridostigmine on gut vagal nerve activity and reduces energy intake. Moreover, our study suggested that the protective effects of pyridostigmine involve nicotine (N)-ACh receptors, as they were not completely abolished by atropine.

Excess lipid accumulation directly alters cellular structures and activates the downstream pathways that lead to cardiomyopathy [13]. In the current study, there was also a remarkable difference in lipid and ceramide deposition between the LV tissues of the NFD and HFD group. Treatment with pyridostigmine reversed these changes and attenuated cardiomyopathy. The possible reasons for this are as follow. First, vagus nerve activation directly reduces lipid accumulation [5]. Thus, pyridostigmine may exert cardioprotective effects by decreasing the accumulation of potentially toxic lipid species. Second, the increase of ACh levels subsequently activates M/N ACh receptors, which play important protective roles in cardiomyocytes. Our previous study showed that ACh mediated M2 receptor activation suppressed hypoxia-induced injury via the MAPK signaling pathway in cardiomyocytes [40]. In our

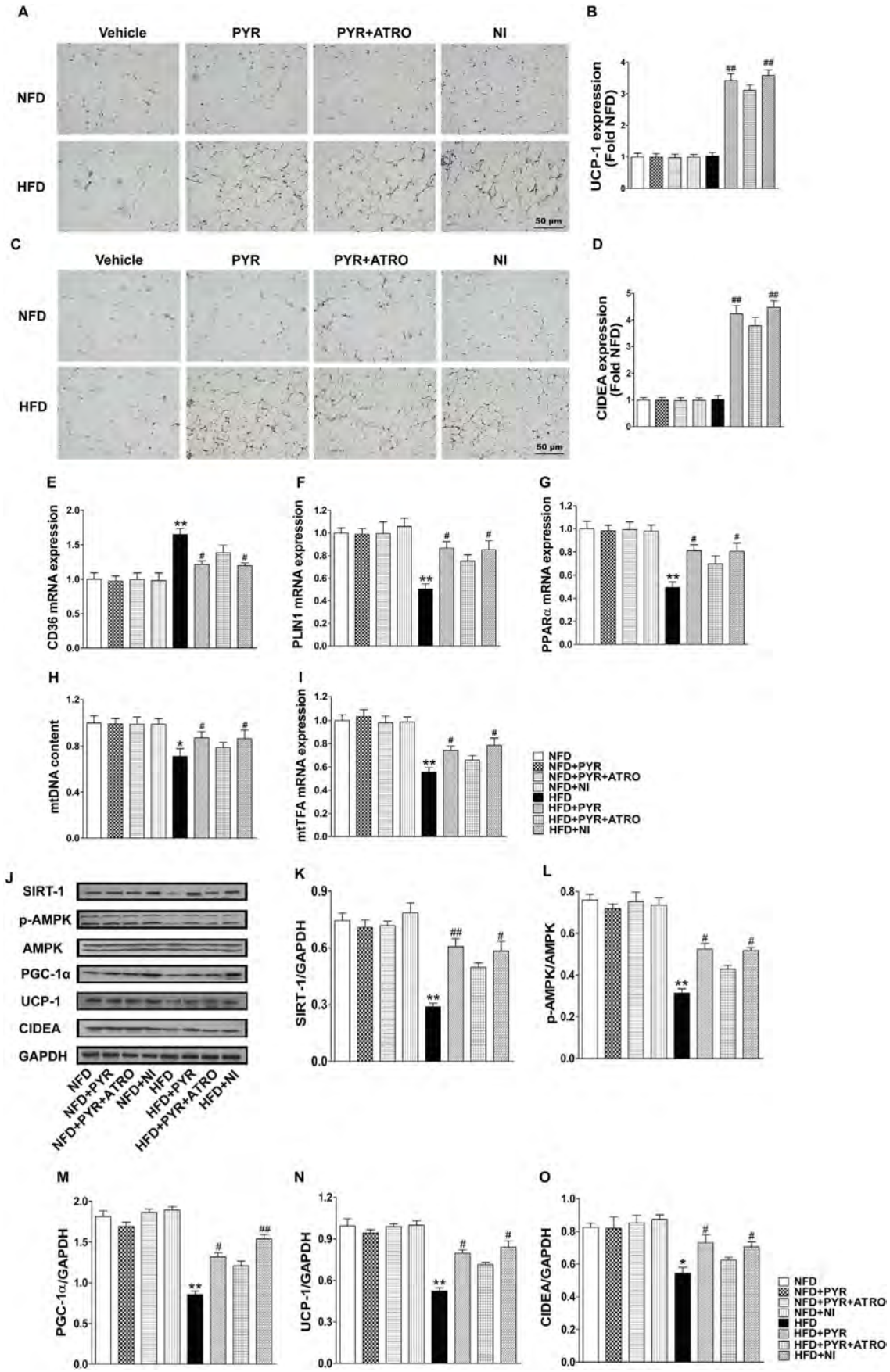

Fig. 6. Pyridostigmine increases WAT browning and BAT activation in HFD rats. (A, C) Representative immunohistochemical staining of UCP-1 and CIDEA in WAT. (B, D) Quantification of UCP-1 and CIDEA levels in WAT. (E–I) CD36, PLIN1, PPARα, mtDNA and mtTFA mRNA levels in WAT. (J) Representative western blots of SIRT-1, p-AMPK, AMPK, PGC-1α, UCP-1 and CIDEA. (K–O) Western blot analysis of SIRT-1, p-AMPK, PGC-1α, UCP-1 and CIDEA expression in BAT. Data are represented as means ± standard error of the mean (n = 8). $^{*}p < 0.05$, $^{**}p < 0.01$ vs. NFD. $^{\#}p < 0.05$, $^{\#\#}p < 0.01$ vs. HFD.

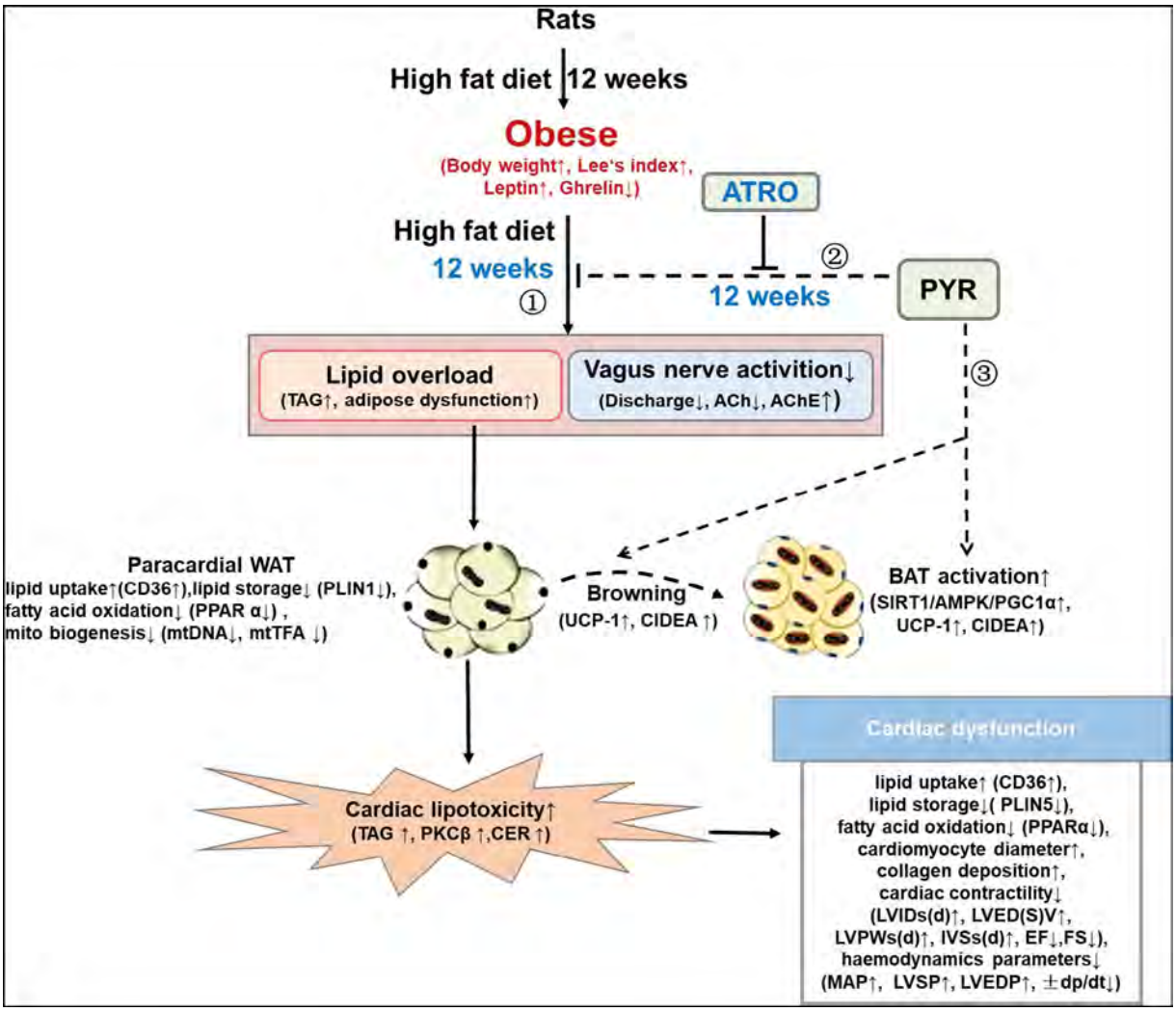

Fig. 7. Pyridostigmine decreases cardiomyopathy by inducing WAT browning and BAT activation in HFD rats. ① a long-term high-fat diet led to the accumulation of several lipid intermediates related to cardiac toxicity, including TAG and ceramide, which were associated with the activation of lipid signaling pathways, as well as a remarkable reduction in vagal discharge; these changes ultimately resulted in cardiac dysfunction and hemodynamic impairment. ② pyridostigmine increased the level of ACh by inhibiting AChE activity and reducing the excess deposition of lipid, without affecting vagal discharge; it also attenuated cardiac remodeling, as evidenced by the improvement of lipid utility and the decrease in cardiac hypertrophy and fibrosis. ③ pyridostigmine enhanced WAT browning associated with enhanced lipid uptake, lipid storage, and fatty acid oxidation, and also enhanced BAT activation via up-regulation of the SIRT-1/AMPK/PGC-1α signaling cascade. ACh, acetylcholine; AChE, acetylcholinesterase; ATRO, atropine; BAT, brown adipose tissue; CD36, Cluster of Differentiation 36; CIDEA, cell death-inducing DNA fragmentation factor A-like effector; CER, ceramide; ± dp/dt, maximum slope of systolic pressure increment and diastolic pressure decrement; EF, left ventricular ejection fraction; FS, left ventricular fractional shortening; HFD, high fat diet; HR, heart rate; IVSd(s), thickness of the interventricular septum; LVIDd(s), left ventricular internal dimension in systole and diastole; LVED(S)V, end-systolic and end-diastolic left ventricular volumes; LVPWd(s), thickness of the left ventricular posterior wall in systole and diastole; LVSP, left ventricular pressure; LVEDP, left ventricular end-diastolic pressure; MAP, mean arterial pressure; mtDNA, mitochondrial DNA; mtTFA, mitochondrial transcription factor A; PLIN 1(5), perilipin 1(5); PPARα, peroxisome proliferator-activated receptor α; PYR, pyridostigmine; TAG, triacylglycerol; UCP-1, uncoupling protein-1; WAT, white adipose tissue.

recent study, it was also demonstrated that vagus nerve stimulation exerted cardioprotective effects by improving mitochondrial function via an M3 receptor/CaMKKbeta/AMPK pathway in rats with myocardial ischemia [41]. Meanwhile, the activated N ACh receptor (α7) ameliorated cardiac fibrosis and improved cardiac function in mice with myocardial infarction [42]. Therefore, pyridostigmine may activate vagal signaling pathways by increasing ACh levels, resulting in improved cardiac function in HFD rats [43].

Previous investigations have also identified that excess lipid accumulation induces adipose tissue dysfunction accompanied by chronic inflammation, which greatly limits the ability of adipose to store the excess energy and instead causes ectopic lipid deposition [16]. Our study showed an association between adipose tissue dysfunction and a significant increase in serum TAG in HFD rats. Pyridostigmine reduced serum TAG and improved adipose tissue function. N ACh receptor activation played a critical role in the inhibition of the inflammatory reaction in adipose tissue [44]. Our recent study showed that an increase in ACh level by vagal stimulation triggers peripheral vascular protection via the N ACh receptor (α7) [45]. Pyridostigmine increased the serum ACh level in HFD + PYR rats, suggesting its possible utility for suppressing adipose dysfunction by attenuating the inflammatory response and decreasing lipid deposition.

Our study showed that a high-fat diet led to cardiac remodeling (cardiac hypertrophy and cardiac fibrosis) and cardiac dysfunction, as well as hemodynamic impairment. Treatment with pyridostigmine ameliorated cardiac remodeling and improved cardiac function. Taha et al. showed that the accumulation of toxic lipids and over-activation of lipid signaling pathways led to cardiomyocyte death [46]. Inhibition of palmitate-induced lipid signaling pathway activation exerts myocardial protection [47]. PKCβ is a crucial molecule involved in the activation of lipid signaling pathways. A deficiency of PKCβ attenuates obesity syndrome in *ob/ob* mice [48]. Therefore, the improvement of

cardiac function by pyridostigmine may be mediated by a reduction in lipid accumulation and inhibition of over-activated of lipid signaling pathways in cardiomyopathy. On the other hand, lipid uptake (CD36), lipid storage (PLIN5), and fatty acid oxidation (PPARα) play important roles in increased lipid metabolism and preserved cardiac function [49–51]. Treatment with pyridostigmine decreased CD36 mRNA and restored PLIN5 and PPARα mRNA levels, which indicated that pyridostigmine may improve lipid metabolism and thereby ameliorates cardiac dysfunction. In our study, nicotinic acid, as the positive control drug, also conferred cardioprotection, albeit via a different mechanism than that of pyridostigmine. Nicotinic acid decreases the synthesis of TAG and thereby ameliorates the dyslipidemic condition, and in turn metabolic syndrome [52]. Pyridostigmine, a reversible cholinesterase inhibitor, enhanced vagal nerve activity and thereby reduced TAG levels, ultimately resulting in a loss of body weight. Compared with nicotinic acid, pyridostigmine had a stronger impact on vagal activation and better protected against cardiac dysfunction in high-fat diet-fed rats.

Recent study showed that WAT browning may be a potential therapeutic target against obesity and the metabolic syndrome [21]. Neyrinck et al. found that green tea extracts promoted WAT browning and decreased lipid storage in adipose tissues, leading to an attenuation of obesity [53]. A fast and visible analysis method was established to evaluate WAT browning. F^{18}-fluroro-2deoxy-D-glucose/positron emission tomography (PET FDG) is considered as a key visual technology to estimate adipose tissue browning [54,55]. Chen et al. observed that a high-fat diet resulted in brown adipose dysfunction using PET FDG in obese mice [56]. Leitner et al. further confirmed that whole-body BAT distribution was different between lean and obese young men [57]. Therefore, PET FDG plays a critical role in the observation of adipose tissue browning and estimation of its metabolic capacity. Several studies demonstrated that the process of WAT browning might be mediated by an increase in the levels of the protein markers UCP-1 and CIDEA [58,59]. In the present study, UCP-1 and CIDEA levels in WAT were increased in HFD + PYR rats, which indicated that pyridostigmine facilitated WAT browning. We also found that lipid uptake (CD36), lipid storage (PLIN1), and fatty acid oxidation (PPARα), as well as mitochondrial biogenesis (mtDNA and mtTFA), were abnormal in WAT, but were improved by pyridostigmine. This may be explained by the activation of the vagal signaling pathway that enhanced energy homeostasis [60].

Imran et al. showed that biomarkers of thermogenesis energy consumption in WAT and BAT, such as CIDEA and UCP-1, were up-regulated via the activation of AMPK [61].The activation of BAT via SIRT-1/AMPK/PGC-1α increases the amount of energy expended by non-shivering thermogenesis [22,23]. We found that pyridostigmine not only increased WAT browning, but also activated BAT, via the SIRT-1/AMPK/PGC-1α signaling cascade reaction, thereby inhibiting excess lipid accumulation in LV tissue and improving cardiac function. Our previous study demonstrated that ACh-activated AMPK promotes PGC-1α expression and improves mitochondrial biogenesis [62]. Therefore, pyridostigmine may increase energy expenditure by enhancing the levels of p-AMPK. In fact, WAT-browning mediated metabolic dysfunction [63]. Some recent studies have reported an association between WAT browning and the development and progression of hypermetabolism in cancer and burns [64,65]. Further research is needed to elucidate the potential mechanisms of WAT browning.

In conclusion, our study showed that a high-fat diet led to cardiac remodeling, mediated by the excess accumulation of lipid and associated with decreased vagal discharge. Pyridostigmine inhibited the deposition of toxic lipid intermediates and attenuated cardiomyopathy. Both were related to enhanced serum ACh levels via the suppression of AChE activity. Pyridostigmine also enhanced WAT browning and BAT activation. These results provide support for the development of novel therapeutic strategies involving vagal nerve activation in patients with obesity-related cardiovascular diseases.

Transparency document

The Transparency document associated with this article can be found, in online version.

Sources of funding

This work was supported by grant from National Natural Science Foundation of China (No. 81770293; No. 81473203; No. 91649106). The authors are grateful to Dr. Xi He and Dr. Ming Zhao for helpful discussion and assistance in preparing figures.

Conflict of interest

The authors declared no conflict of interest.

References

[1] C. Arroyo-Johnson, K.D. Mincey, Obesity epidemiology worldwide, Gastroenterol. Clin. N. Am. 45 (2016) 571–579.
[2] M.D. Jensen, D.H. Ryan, C.M. Apovian, J.D. Ard, A.G. Comuzzie, K.A. Donato, F.B. Hu, V.S. Hubbard, J.M. Jakicic, R.F. Kushner, C.M. Loria, B.E. Millen, C.A. Nonas, F.X. Pi-Sunyer, J. Stevens, V.J. Stevens, T.A. Wadden, B.M. Wolfe, S.Z. Yanovski, 2013 AHA/ACC/TOS guideline for the management of overweight and obesity in adults: a report of the American College of Cardiology/American Heart Association Task Force on Practice Guidelines and The Obesity Society, J. Am. Coll. Cardiol. 63 (2014) 2985–3023.
[3] L.J. Chaar, A. Coelho, N.M. Silva, W.L. Festuccia, V.R. Antunes, High-fat diet-induced hypertension and autonomic imbalance are associated with an upregulation of CART in the dorsomedial hypothalamus of mice, Physiol. Rep. 4 (2016).
[4] K. Lim, B. Barzel, S.L. Burke, J.A. Armitage, G.A. Head, Origin of aberrant blood pressure and sympathetic regulation in diet-induced obesity, Hypertension 68 (2016) 491–500.
[5] S. Banni, G. Carta, E. Murru, L. Cordeddu, E. Giordano, F. Marrosu, M. Puligheddu, G. Floris, G.P. Asuni, A.L. Cappai, S. Deriu, P. Follesa, Vagus nerve stimulation reduces body weight and fat mass in rats, PLoS One 7 (2012) e44813.
[6] P.J. Schwartz, G.M. De Ferrari, A. Sanzo, M. Landolina, R. Rordorf, C. Raineri, C. Campana, M. Revera, N. Ajmone-Marsan, L. Tavazzi, A. Odero, Long term vagal stimulation in patients with advanced heart failure: first experience in man, Eur. J. Heart Fail. 10 (2008) 884–891.
[7] S.S. Kong, J.J. Liu, T.C. Hwang, X.J. Yu, Y. Lu, W.J. Zang, Tumour necrosis factor-alpha and its receptors in the beneficial effects of vagal stimulation after myocardial infarction in rats, Clin. Exp. Pharmacol. Physiol. 38 (2011) 300–306.
[8] S.M. Serra, R.V. Costa, D.C.R. Teixeira, S.S. Xavier, A.C. Nobrega, Cholinergic stimulation improves autonomic and hemodynamic profile during dynamic exercise in patients with heart failure, J. Card. Fail. 15 (2009) 124–129.
[9] M. Gavioli, A. Lara, P.W. Almeida, A.M. Lima, D.D. Damasceno, C. Rocha-Resende, M. Ladeira, R.R. Resende, P.M. Martinelli, M.B. Melo, P.C. Brum, M.A. Fontes, S.R. Souza, M.A. Prado, S. Guatimosim, Cholinergic signaling exerts protective effects in models of sympathetic hyperactivity-induced cardiac dysfunction, PLoS One 9 (2014) e100179.
[10] Y. Lu, J.J. Liu, X.Y. Bi, X.J. Yu, S.S. Kong, F.F. Qin, J. Zhou, W.J. Zang, Pyridostigmine ameliorates cardiac remodeling induced by myocardial infarction via inhibition of the transforming growth factor-beta1/TGF-beta1-activated kinase pathway, J. Cardiovasc. Pharmacol. 63 (2014) 412–420.
[11] Y. Lu, M. Zhao, J.J. Liu, X. He, X.J. Yu, L.Z. Liu, L. Sun, L.N. Chen, W.J. Zang, Long-term administration of pyridostigmine attenuates pressure overload-induced cardiac hypertrophy by inhibiting calcineurin signalling, J. Cell. Mol. Med. 21 (2017) 2106–2116.
[12] K. D'Souza, C. Nzirorera, P.C. Kienesberger, Lipid metabolism and signaling in cardiac lipotoxicity, Biochim. Biophys. Acta 1861 (2016) 1513–1524.
[13] K. Drosatos, P.C. Schulze, Cardiac lipotoxicity: molecular pathways and therapeutic implications, Curr. Heart Fail. Rep. 10 (2013) 109–121.
[14] R.T. Birse, R. Bodmer, Lipotoxicity and cardiac dysfunction in mammals and drosophila, Crit. Rev. Biochem. Mol. Biol. 46 (2011) 376–385.
[15] T. Pulinilkunnil, P.C. Kienesberger, J. Nagendran, T.J. Waller, M.E. Young, E.E. Kershaw, G. Korbutt, G. Haemmerle, R. Zechner, J.R. Dyck, Myocardial adipose triglyceride lipase overexpression protects diabetic mice from the development of lipotoxic cardiomyopathy, Diabetes 62 (2013) 1464–1477.
[16] S.H. Kim, J.P. Despres, K.K. Koh, Obesity and cardiovascular disease: friend or foe? Eur. Heart J. 37 (2016) 3560–3568.
[17] M. Ueno, J. Suzuki, M. Hirose, S. Sato, M. Imagawa, Y. Zenimaru, S. Takahashi, S. Ikuyama, T. Koizumi, T. Konoshita, F.B. Kraemer, T. Ishizuka, Cardiac overexpression of perilipin 2 induces dynamic steatosis: prevention by hormone-sensitive lipase, Am. J. Physiol. Endocrinol. Metab. (2017) 98–2017.
[18] S.S. Choe, J.Y. Huh, I.J. Hwang, J.I. Kim, J.B. Kim, Adipose tissue remodeling: its role in energy metabolism and metabolic disorders, Front. Endocrinol. (Lausanne) 7 (2016) 30.
[19] J. Sanchez-Gurmaches, C.M. Hung, D.A. Guertin, Emerging complexities in adipocyte origins and identity, Trends Cell Biol. 26 (2016) 313–326.

[20] Y. Nishimoto, Y. Tamori, CIDE family-mediated unique lipid droplet morphology in white adipose tissue and brown adipose tissue determines the adipocyte energy metabolism, J. Atheroscler. Thromb. 24 (2017) 989–998.
[21] J. Zuo, D. Zhao, N. Yu, X. Fang, Q. Mu, Y. Ma, F. Mo, R. Wu, R. Ma, L. Wang, R. Zhu, H. Liu, D. Zhang, S. Gao, Cinnamaldehyde ameliorates diet-induced obesity in mice by inducing browning of white adipose tissue, Cell. Physiol. Biochem. 42 (2017) 1514–1525.
[22] P. Baskaran, V. Krishnan, K. Fettel, P. Gao, Z. Zhu, J. Ren, B. Thyagarajan, TRPV1 activation counters diet-induced obesity through sirtuin-1 activation and PRDM-16 deacetylation in brown adipose tissue, Int. J. Obes. 41 (2017) 739–749.
[23] P. Manna, A.E. Achari, S.K. Jain, Vitamin D supplementation inhibits oxidative stress and upregulate SIRT1/AMPK/GLUT4 cascade in high glucose-treated 3T3L1 adipocytes and in adipose tissue of high fat diet-fed diabetic mice, Arch. Biochem. Biophys. 615 (2017) 22–34.
[24] Y. Lu, H. Li, S.W. Shen, Z.H. Shen, M. Xu, C.J. Yang, F. Li, Y.B. Feng, J.T. Yun, L. Wang, H.J. Qi, Swimming exercise increases serum irisin level and reduces body fat mass in high-fat-diet fed Wistar rats, Lipids Health Dis. 15 (2016) 93.
[25] J. Xiao, Y. Bei, J. Liu, J. Dimitrova-Shumkovska, D. Kuang, Q. Zhou, J. Li, Y. Yang, Y. Xiang, F. Wang, C. Yang, W. Yang, miR-212 downregulation contributes to the protective effect of exercise against non-alcoholic fatty liver via targeting FGF-21, J. Cell. Mol. Med. 20 (2016) 204–216.
[26] J.I. Glendinning, J.C. Smith, Consistency of meal patterns in laboratory rats, Physiol. Behav. 56 (1994) 7–16.
[27] M.E. Barbosa, N. Alenina, M. Bader, Induction and analysis of cardiac hypertrophy in transgenic animal models, Methods Mol. Med. 112 (2005) 339–352.
[28] T.P. Fitzgibbons, M.P. Czech, Epicardial and perivascular adipose tissues and their influence on cardiovascular disease: basic mechanisms and clinical associations, J. Am. Heart Assoc. 3 (2014) e582.
[29] S.W. Holwerda, L.C. Vianna, R.M. Restaino, K. Chaudhary, C.N. Young, P.J. Fadel, Arterial baroreflex control of sympathetic nerve activity and heart rate in patients with type 2 diabetes, Am. J. Physiol. Heart Circ. Physiol. 311 (2016) H1170–H1179.
[30] N.E. Straznicky, M.T. Grima, C.I. Sari, E.A. Lambert, S.E. Phillips, N. Eikelis, J.A. Mariani, D. Kobayashi, D. Hering, J.B. Dixon, G.W. Lambert, Comparable attenuation of sympathetic nervous system activity in obese subjects with normal glucose tolerance, impaired glucose tolerance, and treatment naive type 2 diabetes following equivalent weight loss, Front. Physiol. 7 (2016) 516.
[31] S.A. Khan, M. Sattar, N.A. Abdullah, H.A. Rathore, A. Ahmad, M.H. Abdulla, E.J. Johns, Improvement in baroreflex control of renal sympathetic nerve activity in obese Sprague Dawley rats following immunosuppression, Acta Physiol (Oxford) 221 (4) (2017) 250–265.
[32] K. Gil, A. Bugajski, M. Kurnik, P. Thor, Chronic vagus nerve stimulation reduces body fat, blood cholesterol and triglyceride levels in rats fed a high-fat diet, Folia Med. Cracov. 52 (2012) 79–96.
[33] X. He, M. Zhao, X. Bi, L. Sun, X. Yu, M. Zhao, W. Zang, Novel strategies and underlying protective mechanisms of modulation of vagal activity in cardiovascular diseases, Br. J. Pharmacol. 172 (2015) 5489–5500.
[34] A.S. Androne, K. Hryniewicz, R. Goldsmith, A. Arwady, S.D. Katz, Acetylcholinesterase inhibition with pyridostigmine improves heart rate recovery after maximal exercise in patients with chronic heart failure, Heart 89 (2003) 854–858.
[35] J.G. Burneo, E. Faught, R. Knowlton, R. Morawetz, R. Kuzniecky, Weight loss associated with vagus nerve stimulation, Neurology 59 (2002) 463–464.
[36] A. Abubakr, I. Wambacq, Long-term outcome of vagus nerve stimulation therapy in patients with refractory epilepsy, J. Clin. Neurosci. 15 (2008) 127–129.
[37] G.J. Schwartz, The role of gastrointestinal vagal afferents in the control of food intake: current prospects, Nutrition 16 (2000) 866–873.
[38] K. Gil, A. Bugajski, P. Thor, Electrical vagus nerve stimulation decreases food consumption and weight gain in rats fed a high-fat diet, J. Physiol. Pharmacol. 62 (2011) 637–646.
[39] P.P. Soares, N.A. Da, M.R. Ushizima, M.C. Irigoyen, Cholinergic stimulation with pyridostigmine increases heart rate variability and baroreflex sensitivity in rats, Auton. Neurosci. 113 (2004) 24–31.
[40] D.L. Li, J.J. Liu, B.H. Liu, H. Hu, L. Sun, Y. Miao, H.F. Xu, X.J. Yu, X. Ma, J. Ren, W.J. Zang, Acetylcholine inhibits hypoxia-induced tumor necrosis factor-alpha production via regulation of MAPKs phosphorylation in cardiomyocytes, J. Cell. Physiol. 226 (2011) 1052–1059.
[41] R.Q. Xue, L. Sun, X.J. Yu, D.L. Li, W.J. Zang, Vagal nerve stimulation improves mitochondrial dynamics via an M3 receptor/CaMKKbeta/AMPK pathway in isoproterenol-induced myocardial ischaemia, J. Cell. Mol. Med. 21 (2017) 58–71.
[42] Y.H. Yang, H.L. Fang, M. Zhao, X.L. Wei, N. Zhang, S. Wang, Y. Lu, X.J. Yu, L. Sun, X. He, D.L. Li, J.J. Liu, W.J. Zang, Specific alpha7 nicotinic acetylcholine receptor agonist ameliorates isoproterenol-induced cardiac remodelling in mice through TGF-beta1/Smad3 pathway, Clin. Exp. Pharmacol. Physiol. 44 (2017) 1192–1200.
[43] J.J. Liu, N. Huang, Y. Lu, M. Zhao, X.J. Yu, Y. Yang, Y.H. Yang, W.J. Zang, Improving vagal activity ameliorates cardiac fibrosis induced by angiotensin II: in vivo and in vitro, Sci. Rep. 5 (2015) 17108.
[44] A. Gochberg-Sarver, M. Kedmi, M. Gana-Weisz, A. Bar-Shira, A. Orr-Urtreger, Tnfalpha, Cox2 and AdipoQ adipokine gene expression levels are modulated in murine adipose tissues by both nicotine and nACh receptors containing the beta2 subunit, Mol. Genet. Metab. 107 (2012) 561–570.
[45] M. Zhao, X. He, X.Y. Bi, X.J. Yu, W.W. Gil, W.J. Zang, Vagal stimulation triggers peripheral vascular protection through the cholinergic anti-inflammatory pathway in a rat model of myocardial ischemia/reperfusion, Basic Res. Cardiol. 108 (2013) 345.
[46] T. Haffar, A. Akoumi, N. Bousette, Lipotoxic palmitate impairs the rate of beta-oxidation and citric acid cycle flux in rat neonatal cardiomyocytes, Cell. Physiol. Biochem. 40 (2016) 969–981.
[47] A. Sakamoto, M. Saotome, P. Hasan, T. Satoh, H. Ohtani, T. Urushida, H. Katoh, H. Satoh, H. Hayashi, Eicosapentaenoic acid ameliorates palmitate-induced lipotoxicity via the AMP kinase/dynamin-related protein-1 signaling pathway in differentiated H9c2 myocytes, Exp. Cell Res. 351 (2017) 109–120.
[48] W. Huang, R.R. Bansode, N.C. Bal, M. Mehta, K.D. Mehta, Protein kinase Cbeta deficiency attenuates obesity syndrome of ob/ob mice by promoting white adipose tissue remodeling, J. Lipid Res. 53 (2012) 368–378.
[49] Y. Zhang, M. Bao, M. Dai, X. Wang, W. He, T. Tan, D. Lin, W. Wang, Y. Wen, R. Zhang, Cardiospecific CD36 suppression by lentivirus-mediated RNA interference prevents cardiac hypertrophy and systolic dysfunction in high-fat-diet induced obese mice, Cardiovasc. Diabetol. 14 (2015) 69.
[50] H. Wang, U. Sreenivasan, H. Hu, A. Saladino, B.M. Polster, L.M. Lund, D.W. Gong, W.C. Stanley, C. Sztalryd, Perilipin 5, a lipid droplet-associated protein, provides physical and metabolic linkage to mitochondria, J. Lipid Res. 52 (2011) 2159–2168.
[51] A. Elezaby, A.L. Sverdlov, V.H. Tu, K. Soni, I. Luptak, F. Qin, M. Liesa, O.S. Shirihai, J. Rimer, J.E. Schaffer, W.S. Colucci, E.J. Miller, Mitochondrial remodeling in mice with cardiomyocyte-specific lipid overload, J. Mol. Cell. Cardiol. 79 (2015) 275–283.
[52] W.L. Song, G.A. FitzGerald, Niacin, an old drug with a new twist, J. Lipid Res. 54 (2013) 2586–2594.
[53] A.M. Neyrinck, L.B. Bindels, L. Geurts, M. Van Hul, P.D. Cani, N.M. Delzenne, A polyphenolic extract from green tea leaves activates fat browning in high-fat-diet-induced obese mice, J. Nutr. Biochem. 49 (2017) 15–21.
[54] M. Hibi, S. Oishi, M. Matsushita, T. Yoneshiro, T. Yamaguchi, C. Usui, K. Yasunaga, Y. Katsuragi, K. Kubota, S. Tanaka, M. Saito, Brown adipose tissue is involved in diet-induced thermogenesis and whole-body fat utilization in healthy humans, Int. J. Obes. 40 (2016) 1655–1661.
[55] X. Shao, W. Yang, X. Shao, C. Qiu, X. Wang, Y. Wang, The role of active brown adipose tissue (aBAT) in lipid metabolism in healthy Chinese adults, Lipids Health Dis. 15 (2016) 138.
[56] Y. Chen, J. Yang, X. Nie, Z. Song, Y. Gu, Effects of bariatric surgery on change of brown adipocyte tissue and energy metabolism in obese mice, Obes. Surg. (2017), http://dx.doi.org/10.1007/s11695-017-2899-8 [Epub ahead of print].
[57] B.P. Leitner, S. Huang, R.J. Brychta, C.J. Duckworth, A.S. Baskin, S. McGehee, I. Tal, W. Dieckmann, G. Gupta, G.M. Kolodny, K. Pacak, P. Herscovitch, A.M. Cypess, K.Y. Chen, Mapping of human brown adipose tissue in lean and obese young men, Proc. Natl. Acad. Sci. U. S. A. 114 (2017) 8649–8654.
[58] L. Shu, R.L. Hoo, X. Wu, Y. Pan, I.P. Lee, L.Y. Cheong, S.R. Bornstein, X. Rong, J. Guo, A. Xu, A-FABP mediates adaptive thermogenesis by promoting intracellular activation of thyroid hormones in brown adipocytes, Nat. Commun. 8 (2017) 14147.
[59] E. Garcia-Ruiz, B. Reynes, R. Diaz-Rua, E. Ceresi, P. Oliver, A. Palou, The intake of high-fat diets induces the acquisition of brown adipocyte gene expression features in white adipose tissue, Int. J. Obes. 39 (2015) 1619–1629.
[60] D.J. Li, J. Liu, X. Hua, H. Fu, F. Huang, Y.B. Fei, W.J. Lu, F.M. Shen, P. Wang, Nicotinic acetylcholine receptor alpha7 subunit improves energy homeostasis and inhibits inflammation in nonalcoholic fatty liver disease, Metabolism 79 (2017) 52–63.
[61] K.M. Imran, N. Rahman, D. Yoon, M. Jeon, B.T. Lee, Y.S. Kim, Cryptotanshinone promotes commitment to the brown adipocyte lineage and mitochondrial biogenesis in C3H10T1/2 mesenchymal stem cells via AMPK and p38-MAPK signaling, Biochim. Biophys. Acta 1862 (2017) 1110–1120.
[62] L. Sun, M. Zhao, X.J. Yu, H. Wang, X. He, J.K. Liu, W.J. Zang, Cardioprotection by acetylcholine: a novel mechanism via mitochondrial biogenesis and function involving the PGC-1alpha pathway, J. Cell. Physiol. 228 (2013) 1238–1248.
[63] A. Abdullahi, M.G. Jeschke, White adipose tissue browning: a double-edged sword, Trends Endocrinol. Metab. 27 (2016) 542–552.
[64] M. Petruzzelli, M. Schweiger, R. Schreiber, R. Campos-Olivas, M. Tsoli, J. Allen, M. Swarbrick, S. Rose-John, M. Rincon, G. Robertson, R. Zechner, E.F. Wagner, A switch from white to brown fat increases energy expenditure in cancer-associated cachexia, Cell Metab. 20 (2014) 433–447.
[65] L.S. Sidossis, C. Porter, M.K. Saraf, E. Borsheim, R.S. Radhakrishnan, T. Chao, A. Ali, M. Chondronikola, R. Mlcak, C.C. Finnerty, H.K. Hawkins, T. Toliver-Kinsky, D.N. Herndon, Browning of subcutaneous white adipose tissue in humans after severe adrenergic stress, Cell Metab. 22 (2015) 219–227.